The Value of Coarse-Scale Soil Moisture Observations for Regional Surface Energy Balance Modeling

WADE T. CROW AND ERIC F. WOOD

Department of Civil and Environmental Engineering, Princeton University, Princeton, New Jersey

(Manuscript received 23 July 2001, in final form 10 March 2002)

ABSTRACT

Using high-resolution (1 km) hydrologic modeling of the 575 000-km^2 Red–Arkansas River basin, the impact of spatially aggregating soil moisture imagery up to the footprint scale (32–64 km) of spaceborne microwave radiometers on regional-scale prediction of surface energy fluxes is examined. While errors in surface energy fluxes associated with the aggregation of soil moisture are potentially large ($>$50 W m^{-2}), relatively simple representations of subfootprint-scale variability are capable of substantially reducing the impact of soil moisture aggregation on land surface model energy flux predictions. This suggests that even crude representations of subgrid soil moisture statistics obtained from statistical downscaling procedures can aid regional-scale surface energy flux prediction. One possible soil moisture downscaling procedure, based on an assumption of spatial scaling (i.e., a power-law relationship between statistical moments and scale), is demonstrated to improve TOPmodel-based Land–Atmosphere Transfer Scheme (TOPLATS) prediction of grid-scale surface energy fluxes derived from coarse-resolution soil moisture imagery.

1. Introduction

Growing evidence suggests that the accurate representation of surface soil moisture conditions in the land surface component of weather prediction models can improve the predictive abilities of such models within midcontinental areas like the Southern Great Plains (SGP) region of the United States (Koster et al. 2000). This potential has spurred interest in developing a capacity to measure surface soil moisture from space. However, the sharp contrast between the fine spatial scales at which surface soil moisture fields exhibit heterogeneity ($<$100 m) (Famiglietti et al. 1999) and the coarse-resolution scales at which current microwave antennae technology allows for observation of soil moisture from space ($>$50 km) (Jackson et al. 1999) poses a challenge to develop, and clearly demonstrate the value of, a large-scale monitoring system for surface soil moisture. The scaling problem is twofold. First, land surface heterogeneity, in concert with nonlinearities in the spaceborne soil moisture–retrieval process, is capable of introducing error in footprint-scale soil moisture products derived from spaceborne microwave sensors (Njoku et al. 1996; Drusch et al. 1999a,b; Crow et al. 2001). Second, even if footprint-scale representations of soil moisture are free from error, the loss of subfootprint-scale heterogeneity may degrade the utility of such representations for weather and seasonal climate prediction.

The second impact can be further subdivided into two separate effects. Given modeling evidence that suggests that sharp horizontal gradients in the land surface energy balance can induce organized mesoscale circulations (OMCs) (Lynn et al. 1995; Seth and Giorgi 1996; Weaver and Avissar 2001), the loss of soil moisture spatial heterogeneity can potentially degrade the representation of mesoscale circulations in weather prediction models. Following Giorgi and Avissar (1997), this impact is referred to as the ''dynamic'' effect of land surface heterogeneity. The second potential impact on weather prediction, referred to as the ''aggregation'' effect by Giorgi and Avissar (1997), occurs when heterogeneous land surface parameters or state variables (such as soil moisture) are processed through nonlinear model physics to obtain predictions of land surface water and energy fluxes. This variability, the dynamic effects of which are effectively homogenized by the planetary boundary layer, does not produce a coherent atmospheric response. Nevertheless, nonlinear relationships between land surface variables and many surface fluxes dictate that grid-scale predictions of fluxes will be sensitive to the presence, or absence, of subgrid-scale variability. Discussions of aggregation effects within the SGP region often center on soil moisture because of its critical role in driving the surface energy balance within the region (Gupta et al. 1999), its nonlinear relationship with many land surface fluxes (Wetzel and Chang 1987), and the

Corresponding author address: Dr. Wade T. Crow, Hydrology and Remote Sensing Laboratory, ARS/USDA, Beltsville, MD 20705.
E-mail: wcrow@hydrolab.arsusda.gov

large range of spatial scales at which it has been observed to exhibit heterogeneity (Rodriguez-Iturbe et al. 1995; Crow et al. 2000).

Neither impact, dynamic or aggregation, has been definitively shown to affect weather prediction within the SGP region. The ability of land surface heterogeneity to generate significant atmospheric circulations (i.e., the dynamic effect) appears highly dependent on synoptic conditions (Fast and McCorcle 1991), and at least some modeling evidence suggests that realistic patterns of land surface heterogeneity do not yield significant OMCs (Zhong and Doran 1997, 1998). In addition, the generation of OMCs is typically associated with heterogeneity at length scales coarser than 10 km (Avissar and Schmidt 1998) and is therefore potentially resolvable if synthetic aperture radiometry technology is utilized in next-generation antennae design for microwave remote sensors (Le Vine et al. 1994). In terms of the aggregation effect, Wetzel and Chang (1988), Famiglietti and Wood (1995), and Wood (1997) all argue for a large impact associated with the spatial aggregation of soil moisture, while contrary conclusions are presented by Sellers et al. (1995) and Kustas and Jackson (1999).

In cases where land surface aggregation effects are large, subgrid land surface heterogeneity can be incorporated into land surface models through a probability density function (PDF) representation. The PDF approach has been used for soil moisture, or surrogates for soil moisture, such as stomatal conductance, in a number of land surface schemes (Wetzel and Chang 1988; Avissar 1992; Famiglietti and Wood 1994b; Wetzel and Boone 1995). However, if the grid scale corresponds to the footprint scale at which soil moisture information is available, estimating subgrid statistics is not a trivial task. Estimation of subgrid statistics in this case requires a ''downscaling'' strategy capable of connecting fine-scale variability to observable magnitudes of coarse-scale heterogeneity (Blöschl and Sivipalan 1995). One possible downscaling approach is to assume that the statistical moments of soil moisture fields have a power-law relationship with scale, and to estimate magnitudes of fine-scale (or subresolution scale) variability based on fitting a scaling exponent to observed coarse-scale field statistics and extrapolating to finer scales (Dubayah et al. 1997).

The value of coarse-scale surface wetness observations for energy balance modeling depends both on the magnitude of the aggregation and dynamic impacts associated with smoothing soil moisture and the feasibility of strategies to correct modeling errors associated with each impact. This paper focuses on the soil moisture aggregation impact. Using TOPmodel-based Land–Atmosphere Transfer Scheme (TOPLATS) simulations over the SGP region, this analysis will quantify the magnitude of the soil moisture aggregation effect on the coarse-scale prediction of land surface energy fluxes and assess the ability of the downscaling strategy introduced by Dubayah et al. (1997) to compensate surface energy flux predictions for the impact of nonresolved soil moisture heterogeneity.

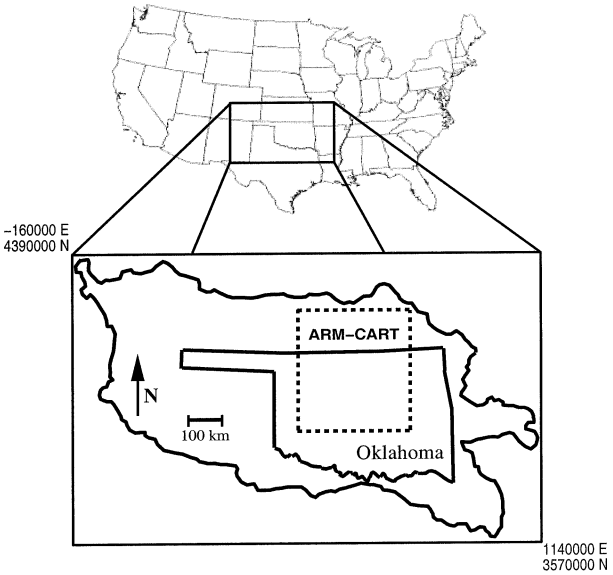

FIG. 1. Location of Red–Arkansas River basin and ARM CART study site within the U.S. SGP.

2. TOPLATS modeling

TOPLATS modeling of the SGP region was used to generate realistically heterogeneous soil moisture fields. For a full description of TOPLATS see Famiglietti and Wood (1994b) and Peters-Lidard et al. (1997). Simulations were run on a 1-km modeling grid over the 575 000-km^2 Red–Arkansas River basin during the 1994 growing season (0100 UTC 1 April 1994–2400 UTC 31 July 1994). See Fig. 1 for location and scale of the basin. Hourly precipitation products were obtained from 4-km estimates of hourly rainfall accumulations retrieved by the Next Generation Weather Radar (NEXRAD) system of Weather Surveillance Radar-1988 Doppler (WSR-88D) radars (Hudlow et al. 1991). Incoming solar radiation imagery was derived from processing 1-km Geostationary Operational Environmental Satellite (GOES) imagery of reflected solar radiation through the 2001 shortwave radiative transfer algorithm (Diak and Gautier 1983). Surface meteorology data (e.g., wind speed, air pressure, surface temperature, and wet-bulb surface temperature) were taken from the spatial interpolation of measurements made at 72 National Climate Data Center (NCDC) stations within the south-central United States. Land cover was taken from a 1-km classification map derived from Advanced Very High Resolution Radiometer (AVHRR) imagery of the SGP region. Soil and topographic information was based on 1-km imagery of depth-to-bedrock estimations, a 1-km State Soil Geographic (STATSGO) soil texture image, and a 1-km U.S. Department of Agri-

TABLE 1. Vegetation parameters used in TOPLATS modeling where, f_{sz} is the fraction of root area in the surface zone. Surface albedo (α) values were taken from Pielke (1984), Stull (1995), and Dingman (1994). Surface emissivity (ϵ) values were taken from Brutsaert (1982). Momentum roughness (z_{0m}) values were taken from Brutsaert (1982) and Pielke (1984). Following Betts and Beljaars (1993), roughness lengths for heat transport (z_{0h}) were assigned to be $0.01*z_{0m}$. Based on recommendations made by Kondo (1971), values of zero place desplacement (d) for trees and shrubs were set equal to ⅔ of assumed vegetation height.

Vegetation type	f_{sz}	α	ϵ	z_{0m} (m)	d (m)
Crop	0.40	0.24	0.96	0.05	0.0
Short grass	0.40	0.24	0.96	0.02	0.0
Tall grass	0.20	0.20	0.95	0.05	0.0
Deciduous trees	0.00	0.20	0.96	0.15	0.6
Coniferous trees	0.00	0.15	0.96	0.15	0.6
Deciduous shrub	0.40	0.20	0.96	0.10	0.4
Coniferous shrub	0.40	0.15	0.96	0.10	0.4
Water	n/a	0.15	0.98	0.005	0.0

TABLE 2. Vegetation parameters used in TOPLATS modeling. Leaf area index (LAI) values were based on values listed in Pielke (1984). Minimum stomatal resistance (r_s, min) values were based on values listed in Peters-Lidard et al. (1997). Following Jacquemin and Noilhan (1990), maximum stomatal conductance (r_s, max) was set equal to 5000 m s^{-1} for all species. The root spacing parameter (b) is described in Feddes and Rijtema (1972). Internal plant resistance (R_p) values were based on values calculated by Federer (1979), Choudhury and Federer (1984), and Choudhury and Idso (1985). Following Wetzel and Chang (1987), the wilting soil water potential at which vegetation close their stomata was taken to be −2.1 MPa for all vegetation types.

Vegetation type	LAI Max	LAI Min	r_s, min (m s^{-1})	b (m)	R_p (s)
Crop	2.0	0.5	80.0	0.001	6×10^8
Short grass	2.0	0.5	40.0	0.001	6×10^8
Tall grass	2.0	0.5	40.0	0.001	6×10^8
Deciduous trees	3.0	1.0	120.0	0.0025	1.2×10^9
Coniferous trees	3.0	1.0	120.0	0.0025	1.2×10^9
Deciduous shrub	3.0	1.0	80.0	0.0025	1.2×10^9
Coniferous shrub	3.0	1.0	80.0	0.0025	1.2×10^9
Water	0.0	0.0	n/a	n/a	n/a

culture (USDA) digital elevation map (DEM) of the basin. Soil hydrology parameters were taken from Cosby et al. (1984), except for values of saturated hydraulic conductivity, which were based on those listed in Rawls et al. (1982). The following land cover classification categories were used: short grass, agricultural crops, tall grass, deciduous trees, coniferous tress, deciduous shrubs, coniferous shrubs, water, and bare soil. Based on values reported in the literature, Tables 1 and 2 assigned water and energy balance parameters to each of these land cover types. Two soil layers were used: a 15-cm surface zone and a subsurface zone extending from the bottom of the surface zone to the top of the water table.

a. TOPLATS calibration and validation

The period of high-resolution modeling was supported by longer periods of low-resolution modeling for purposes of model calibration and generation of realistic initial conditions. Low-resolution modeling was based on subdivision of the entire Red–Arkansas basin into 314 separate subcatchments. Forcing data for low-resolution modeling was obtained from datasets constructed during phase 2c of the Project for the Intercomparison of Land-Surface Parameterization Schemes (PILPS-2c) study of the Red–Arkansas River basin (Wood et al. 1998).

Calibration of the water balance portion of TOPLATS was based on comparisons of TOPLATS predictions to naturalized streamflow data obtained for five subcatchments in the eastern portion of the basin. The emphasis on the eastern edge of the Red–Arkansas basin is appropriate given that the model processes affected by calibration (i.e., baseflow and saturation excess runoff) are significant only in the eastern portion of the SGP. To obtain realistic initial conditions for high-resolution TOPLATS modeling, the statistical version of TOPLATS was run at an hourly time step over each of the 314 subcatchments from 0100 UTC 1 January 1991 to 2400 UTC 1 March 31 1994.

Point-scale TOPLATS predictions of surface energy flux, surface soil moisture, and surface temperature have been extensively validated within the SGP region (Famiglietti and Wood 1994a; Peters-Lidard et al. 1997, 2001). For the simulations described here, TOPLATS energy flux predictions were validated against measurements made by Energy Balance Bowen Ratio (EBBR) flux towers within the SGP Atmospheric Radiation Measurement Program Cloud and Radiation Test bed (ARM CART) site. Figure 2 compares the spatial average of TOPLATS predictions over the entire ARM CART site to the average of all nine EBBR flux towers. Unambiguous validation of energy flux predictions over such a large spatial scale is extremely difficult, and several points should be acknowledged with regard to validation results presented in Fig. 2. Nine flux tower observations over the entire 140 000-km^2 site represents very sparse spatial sampling. Furthermore, in 1994, all EBBR flux tower sites were located in fields containing pasture or rangeland land cover, suggesting that abundant areas of winter wheat land cover are undersampled in our validation dataset. The overall impact of these sampling limitations on the description of ARM CART site–scale energy fluxes provided by averaging EBBR flux tower observations is unclear. Gao et al. (1998) compare 1-km PASS (PArameterization of Subscale Surface fluxes) model results for the entire ARM CART site to the spatial average of EBBR flux tower measurements available in July 1995 and find close agreement for sensible heat flux (H) magnitudes but a positive bias of 50 W m^{-2} in model predictions of latent heat flux (λE) during the afternoon. They suggest that poor EBBR sampling of the generally wetter eastern half of the ARM CART site contributes to an underestimation of ARM CART site–scale latent heat flux (λE) by the

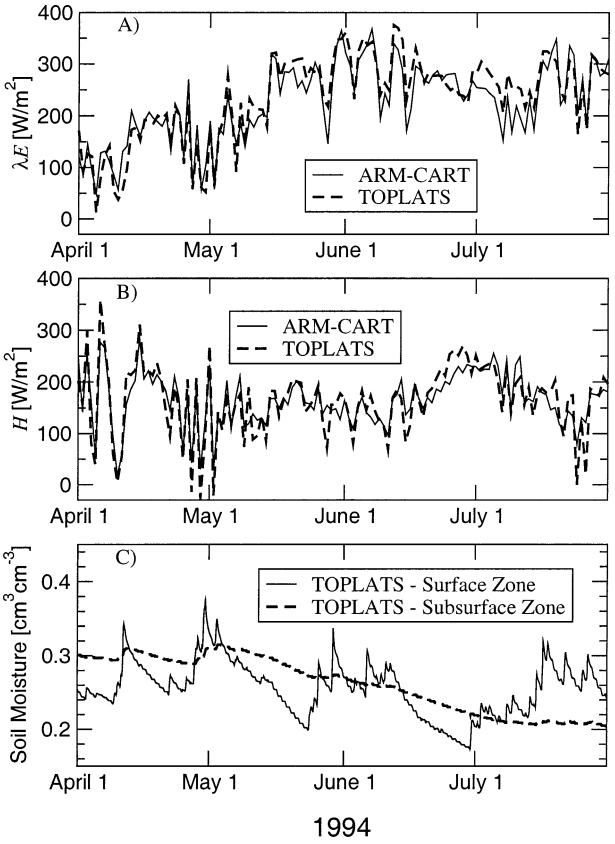

FIG. 2. Time series of modeled (TOPLATS) vs observed levels of ARM CART site–averaged (a) latent (λE) and (b) sensible (H) heat flux. Plotted values are daily averages of observations/predictions made over a 7-h period centered on local solar noon (1900 UTC). Observed values are an average of measurements made at nine bowen ratio flux towers within the ARM CART site. (c) Hourly time series of modeled (TOPLATS) surface and subsurface volumetric soil moistures over the ARM CART site.

EBBR observations. However, for exactly the same time period in summer 1995, Doran et al. (1998) make similar comparisons between averaged EBBR observations and distributed Simple Biosphere Model version 2 (SiB2) predictions and find a positive bias in model predictions of H—implying an overestimation of λE in averaged EBBR observations—throughout the diurnal cycle. They attribute this midsummer bias to the neglect of EBBR observations within fallow winter wheat (i.e., bare soil) fields.

b. Aggregation and reinsertion procedure

Figure 3 shows imagery produced by the 1-km TOPLATS simulations and gives a sense as to the magnitude of land surface heterogeneity predicted by the model. Using TOPLATS, benchmark imagery of 1-km surface and subsurface soil was obtained at every local solar noon (1900 UTC) between 1 April 1994 and 31 July 1994. This soil moisture imagery was linearly aggregated to a coarser footprint scale and, at the appropriate solar noon, reinserted into a second TOPLATS simulation calculated with identical forcings. Footprint scales between 2 and 64 km were examined in this way, but the 1-km computational grid scale and full 1-km variability in other model forcings and parameters were maintained in all simulations. Insertion occurred every local solar noon, and the water and energy balance of TOPLATS was allowed to evolve normally for the 24-h period between image insertions. TOPLATS energy flux predictions for various soil moisture resolutions were compared for time steps immediately following the insertion of coarse-scale imagery to minimize the impact of small-scale soil moisture heterogeneity regenerated by the model. The procedure was designed to mimic the daily insertion of coarse-scale remotely sensed soil moisture observations into a land surface model operating at a finer grid scale.

3. Impact of soil moisture aggregation

Spatial averaging and reinsertion of high-resolution (1 km) TOPLATS soil moisture products back into the energy balance portion of TOPLATS provides an opportunity to simulate the impact of utilizing low-resolution soil moisture observations to make regional-scale surface energy flux predictions within a higher-resolution model. Analytical representations of this impact are straightforward. Let $\theta(x, y)$ represent a continuous two-dimensional field of soil moisture. The mean of $\theta(x, y)$ within a computational grid cell of size λ is

$$\langle\theta\rangle_\lambda = \lambda^{-2}\int\int \theta(x, y)\, dx\, dy = \theta_\lambda, \qquad (1)$$

where the subscript λ represents the footprint scale over which the underlying field is averaged. For convenience, the angled bracket notation is dropped in some expressions, and the presence of a scale subscript alone is used to indicate linear spatial averaging. Using this notation, the difference between utilizing a continuous field moisture field θ and a field averaged up to some grid scale λ to calculate a grid-scale flux F can be summarized by taking the expectation of a Taylor series expansion of $F(\theta)$ around the grid-scale soil moisture θ_λ:

$$\langle F(\theta_\lambda)\rangle_\lambda - \langle F(\theta)\rangle_\lambda = -\sum_{j=1}^{\infty}\frac{1}{j!}\left\langle(\theta - \theta_\lambda)^j\left.\frac{\partial^j F(\theta)}{(\partial\theta)^j}\right|_{\theta_\lambda}\right\rangle_\lambda. \qquad (2)$$

An expansion of Eq. (2) yields

$$\langle F(\theta_\lambda)\rangle_\lambda - \langle F(\theta)\rangle_\lambda = -\sum_{j=2}^{\infty}\frac{1}{j!}\langle(\theta - \theta_\lambda)^j\rangle_\lambda\left\langle\left.\frac{\partial^j F(\theta)}{(\partial\theta)^j}\right|_{\theta_\lambda}\right\rangle_\lambda - \sum_{k=1}^{\infty}\frac{1}{k!}\,\mathrm{cov}\left\{(\theta - \theta_\lambda)^k,\left.\frac{\partial^k F(\theta)}{(\partial\theta)^k}\right|_{\theta_\lambda}\right\}. \qquad (3)$$

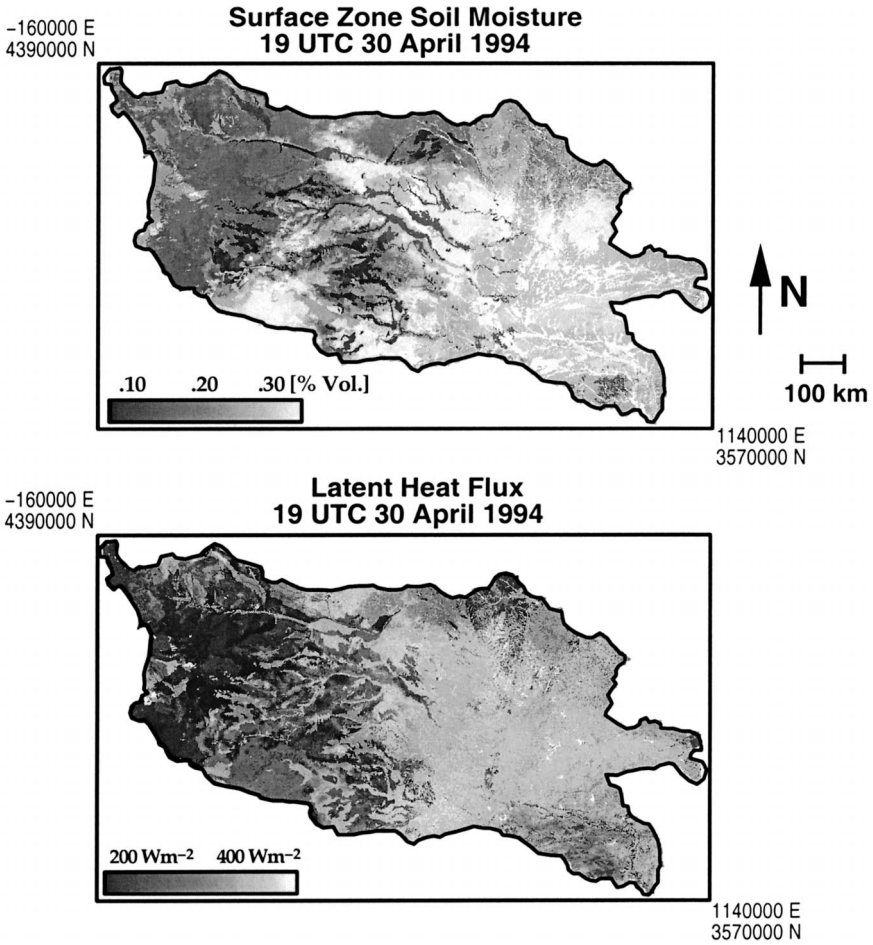

FIG. 3. Typical imagery of surface zone soil moisture and latent heat flux generated by a 1-km TOPLATS simulation of the Red–Arkansas River basin.

The soil moisture aggregation effect is composed of two separate processes. The first term on the right-hand side of Eq. (3) describes how sensitivity to the presence of subgrid-scale soil moisture variability arises from the nonlinearity of F with respect to soil moisture in combination with a significant spread of the local subgrid values θ around the grid-scale mean θ_λ. This term will be referred to as the ''nonlinearity'' term. The second term in Eq. (3) describes the impact of losing correlation between the subgrid field θ and derivatives of the $F(\theta)$ relationship and will be referred to as the ''loss-of-correlation'' term. This term can be neglected for the case of statistical independence between subgrid soil moisture and variations in the relationship between soil water fluxes and soil moisture. However, the point-scale relationship between soil water fluxes (i.e., drainage, evaporation, and transpiration) and soil moisture varies strongly between soil texture and vegetation types (Hillel 1980). These soil water fluxes, in turn, impact expected magnitudes of soil moisture. Therefore, correlation inevitably develops between local soil and vegetation properties, which determine $F(\theta)$, and local soil moisture fluctuations. The loss-of-correlation term describes the net impact on grid-scale fluxes of failing to resolve such correlation. Both terms are derived with the implicit assumption that fine-scale land surface parameters are known and, consequently, neglect impacts associated with the aggregation of such parameters (see, e.g., Boulet et al. 1999).

Model closure for the impact of nonresolved soil moisture heterogeneity on flux estimates depends on the accurate approximation of both terms in Eq. (3) using only grid-scale information. Since higher-order derivatives of the relationship between F and θ are known a priori, the nonlinearity term can be recovered from subgrid-scale statistical information. Furthermore, if a given two-parameter distribution shape can be accurately fit to subgrid soil moisture distributions, all such subgrid statistics are specified by the subgrid soil moisture variance. In contrast, approximation of the loss of correlation term requires a more complex representation of subgrid variability describing the spatial interplay between subgrid model parameters and soil moisture heterogeneity.

4. Soil moisture spatial scaling

Dubayah et al. (1997) and Hu et al. (1998) both note the potential of spatial scaling to provide the basis for a soil moisture downscaling approach. A given field θ is said to scale spatially if its statistical moments, observed at any two spatial resolutions λ and λ_0, obey the following power-law relationship

$$\langle \theta_\lambda^q \rangle = \left(\frac{\lambda}{\lambda_0}\right)^{K(q)} \langle \theta_{\lambda_0}^q \rangle \tag{4}$$

or, equivalently,

$$\log\langle \theta_\lambda^q \rangle = K(q) \log\left(\frac{\lambda}{\lambda_0}\right) + \log\langle \theta_{\lambda_0}^q \rangle, \tag{5}$$

where q is the order of the statistical moment, K is the scaling parameter, and the angled brackets are used to describe spatial averaging. The ratio λ/λ_0 is called the ''scale factor.'' If $\lambda < \lambda_0$, the scale factor is less than one, and Eq. (5) illustrates a downscaling procedure that connects fine-scale (λ) field statistics to coarse-scale (λ_0) information. If $K(q)$ varies linearly with q, the field is said to exhibit ''simple scaling.'' Simple scaling fields therefore exhibit two basic features: log–log linearity in $\langle \theta_\lambda^q \rangle$ versus the scale factor and a linear relationship between the scaling exponents $K(q)$ and the statistical moment q. It is possible for the first requirement to hold, but not the second. Fields are said to exhibit multiscaling if they demonstrate log–log linearity in $\langle \theta_\lambda^q \rangle$ versus the scale factor, but concavity in the relationship between $K(q)$ and q. Multiscaling fields are not strictly self-similar, in the sense that a set of scaling exponents $K(q)$ is required to translate moments between scales (Gupta and Waymire 1990).

As demonstrated by Dubayah et al. (1997), spatial scaling allows for estimation of fine-scale (i.e., nonresolved) variability from coarse-scale (i.e., resolved) soil moisture spatial structure. Figure 4 demonstrates the procedure for the second moment $\langle \theta_\lambda^2 \rangle$ of a typical soil moisture field generated by TOPLATS. Assuming the finest observable to be 32 km, a scaling exponent $K(2)$ can be fitted in log–log space within the resolved range of scales. This exponent is then used to extrapolate down to finer scales, providing an estimate of the sub-32-km variability present in the soil moisture field. Estimates of such fine-scale statistics are required for approximation of the nonlinearity term in Eq. (3). Simple scaling requires only that a single moment be fitted, since the scaling exponent at one moment can be linearly related to any other moment. The procedure is also applicable to multiscaling fields, with the caveat that fitting of a separate scaling exponent $K(q)$ is required for each moment q.

5. Results

Results presented in this section use TOPLATS modeling results (section 2) to quantify the impact of the soil moisture aggregation effect (section 3) on surface energy flux prediction within the SGP region. Based on the downscaling procedure outlined in section 4, a strategy for correcting energy flux predictions for the impact of nonresolved soil moisture heterogeneity is developed.

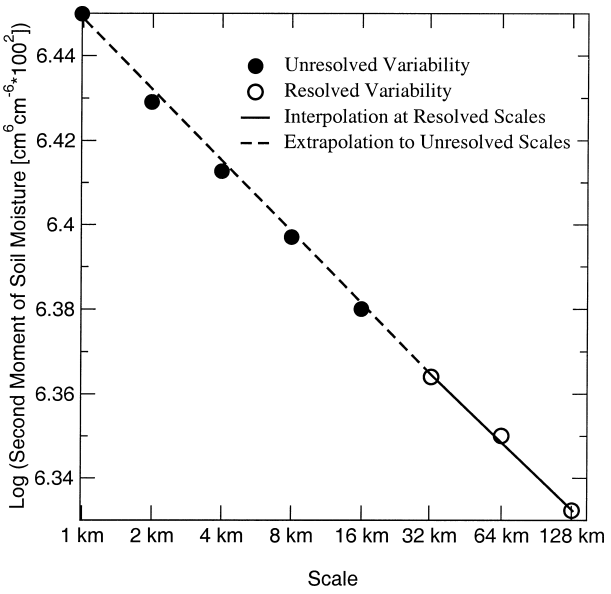

FIG. 4. Schematic of downscaling strategy based on spatial scaling. The strategy is based on fitting a least squares regression line at (resolvable) scales and extrapolating down to finer (unresolvable) scales in order to estimate fine-scale soil moisture statistics (Dubayah et al. 1997).

a. Effect of soil moisture aggregation

Figure 5a shows a time series of biases in TOPLATS surface energy flux predictions for the entire ARM CART site derived from 32-km (versus 1 km) soil moisture information. Coarse-scale (32 km) results are based on noontime predictions made immediately after the insertion of spatially averaged imagery back into TOPLATS. Soil moisture impacts λE by controlling the rate at which water can be extracted from the soil for either evaporation or transpiration. Following Wetzel and Chang (1987), actual evapotranspiration is taken to be the minimum of the threshold evapotranspiration rate λE_T [calculated as a function of soil moisture θ and using the formulation presented in Feddes and Rijtema (1972)] and the potential evapotranspiration rate λE_p [calculated using the Jarvais (1976) type formulation outlined in Peters-Lidard et al. (1997)]. Such ''supply and demand'' formulations for evapotranspiration are a common component of land surface models (Desborough 1997) and have been successfully applied to surface energy flux modeling with the SGP region (Wetzel and Chang 1988; Famiglietti and Wood 1994a; Wetzel and Boone 1995). Typical $\lambda E_T(\theta)$ curves, based on Feddes and Rijtema (1972) and parameters given in Table 2, are shown in Fig. 6. Soil moisture also directly effects

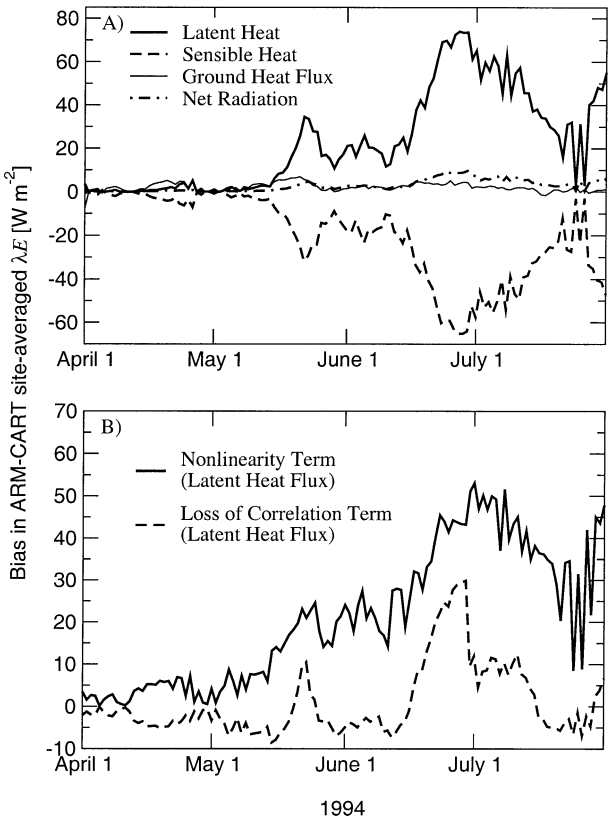

FIG. 5. (a) Net bias of TOPLATS surface energy flux predictions over the ARM CART site derived from 32-km (vs 1 km) soil moisture data and (b) decomposition of bias in latent heat flux into the nonlinearity term and the loss of correlation term described in Eq. (3).

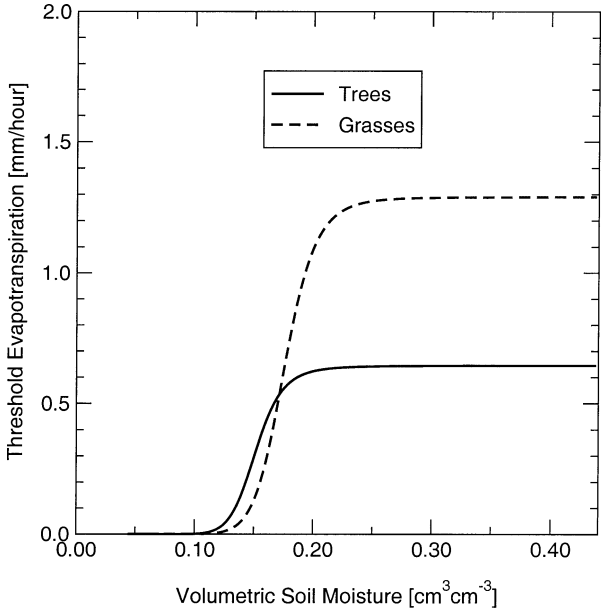

FIG. 6. Relationship between threshold evapotranspiration (λE_T) and soil moisture for trees and grasses in a sandy loam soil.

ground heat flux (G) through its control on the thermal properties of soil (Peters-Lidard et al. 1998). Since the sensitivity of surface albedo on soil wetness is neglected, other components of the energy balance are not directly impacted by soil moisture.

Small (<10 W m^{-2}) errors in G are seen in Fig. 5a throughout the growing season. Much larger errors in λE appear during mid-May, when soil water storage over portions of the ARM CART region is sufficiently depleted to allow for soil moisture control of evapotranspiration. Errors in λE reach a maximum during a particularly dry portion of the growing season in late June and early July (see Fig. 2c). The net soil moisture aggregation impact on λE is always positive, suggesting that degradation of soil moisture resolution from 1 to 32 km biases large-scale calculations of λE high. Among components of the energy balance, errors in λE are largely compensated for by a decrease in sensible heating H. A slight rise in R_n is observed, but it is an order of magnitude smaller than the impact on H and λE. This interplay maximizes the sensitivity of grid-scale Bowen ratio ($H/\lambda E$) predictions to the presence of subgrid-scale soil moisture variability.

Latent heat flux errors shown in Fig. 5a have two separate sources, corresponding to the two terms shown in Eq. (3). Figure 5b shows time series of local noontime (1900 UTC) values for both terms in Eq. (3) averaged over the entire ARM CART site. The nonlinearity term is consistently positive. As shown in Fig. 6, the transpiration–soil moisture function has two distinct regions of concavity, one negative at high soil moistures and one positive at low soil moistures. Following Eq. (3), the consistently positive bias shown in Fig. 5b implies that the region of negative concavity plays a dominant role in determining the sign of the nonlinearity term. This is due to the relative scarcity of 32-km soil moisture values within the region of positive concavity at or just above the wilting point. Soil water loss for moisture levels near wilting is small for bare soil surfaces and effectively zero for vegetated pixels. Consequently, spatial distributions of 1-km soil moisture values tend to become positively skewed for dry conditions, because local soil moisture levels have difficulty progressing far below wilting. This skew makes it dynamically difficult for 32-km average soil moisture values to fall into the regime of positive concavity needed to make the nonlinearity term negative. In contrast, the loss of correlation term varies in sign from negative early in the growing season to positive during drier periods in June and July but is significant only during two relatively dry periods of the simulation (mid- to late May and late June; see Fig. 2c). During these two dry periods, it contributes about one-third of the total error associated with the soil moisture aggregation effect.

Figure 7 plots root-mean-square (rms) error in domain-averaged TOPLATS λE predictions corresponding to insertion of soil moisture products with horizontal resolutions of 1, 2, 4, 8, 16, 32, and 64 km. Error values

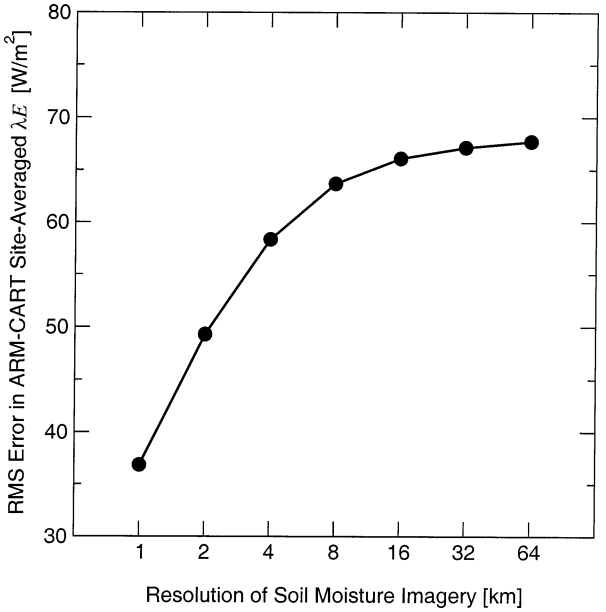

FIG. 7. Error in ARM CART site–averaged latent heat flux TOPLATS predictions (vs the spatial average of flux tower measurements) derived from a range of soil moisture resolutions. Error values plotted are rms errors in local solar noon (1900 UTC) TOPLATS predictions made between 1 Jun and 31 Jul 1994.

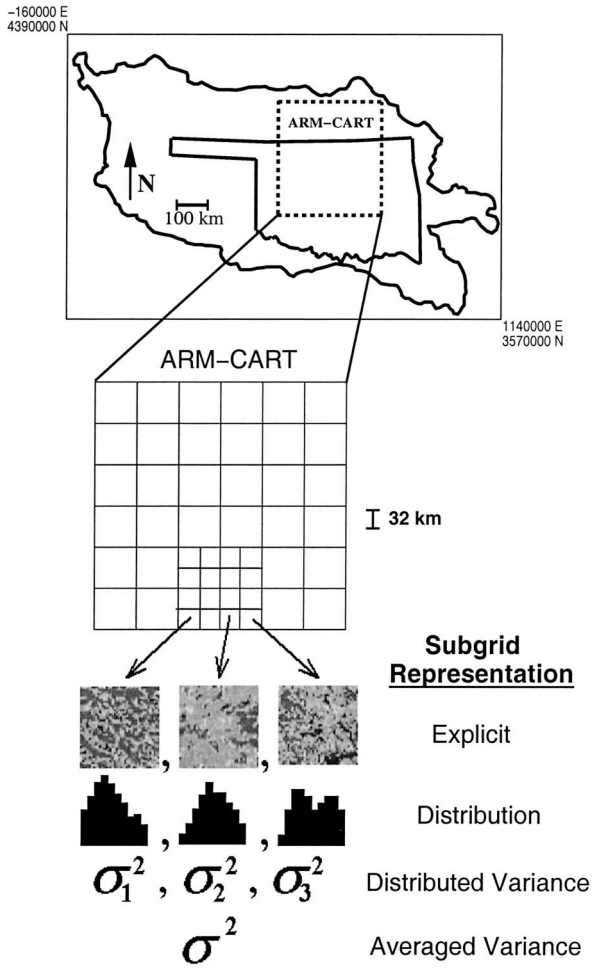

FIG. 8. Various representations of subgrid-scale soil moisture heterogeneity for 32-km grid cells within the ARM CART site.

are for local noontime (1900 UTC) TOPLATS predictions made between 1 June and 31 July 1994 and are calculated relative to validation estimates derived from averaging measurements from EBBR flux towers within the ARM CART study area. Using 1-km soil moisture data, comparisons with flux tower data reveal an rms difference between model and validation values of 36.9 W m^{-2}. This difference rises to 67.1 W m^{-2} as the spatial resolution of soil moisture information used to predict surface energy fluxes flux is degraded from 1 to 64 km. Consequently, nearly half the error incurred when using 64-km soil moisture data is attributable to the neglect of soil moisture spatial variability.

The magnitude of the nonlinearity term shown in Fig. 5b is a direct consequence of nonlinearities in the modeled relationship between soil moisture and evapotranspiration. The supply and demand–type formation employed here (Fig. 6) has a clear physical basis and is commonly used in land surface models. Nevertheless, it represents only one of a number of possible formations. More linear relationships between soil moisture and evapotranspiration would yield smaller magnitudes for the impact of soil moisture aggregation. Therefore, some model dependency must be acknowledged for results in Figs. 6 and 7.

b. Subgrid soil moisture representations

A portion of the error observed in Fig. 7 can be remediated through simplified representations of subgrid soil moisture heterogeneity. Figure 8 demonstrates four separate cases along the continuum of possible representations for subgrid soil moisture heterogeneity within the ARM CART site: explicit representation of the variability, a distribution for each grid cell, a subgrid variance for each grid cell, and a single subgrid variance for the entire model domain. Figure 9a shows the rms errors in ARM CART site–scale λE associated with utilizing each representation in TOPLATS. A fifth case—complete neglect of subgrid-scale variability—is also considered. For the ''distributed variance'' and ''averaged variance'' representations, subgrid soil moisture variability is assumed to follow a beta probability distribution. Errors are calculated relative to both independent ARM CART validation data and benchmark TOPLATS results derived from 1-km soil moisture information.

Relative to benchmark TOPLATS results, degrading soil moisture information from an ''explicit field'' to a ''distribution'' representation introduces an rms error of 11.7 W m^{-2} into local noontime (1900 UTC) TOPLATS predictions of ARM CART site–averaged λE. This error

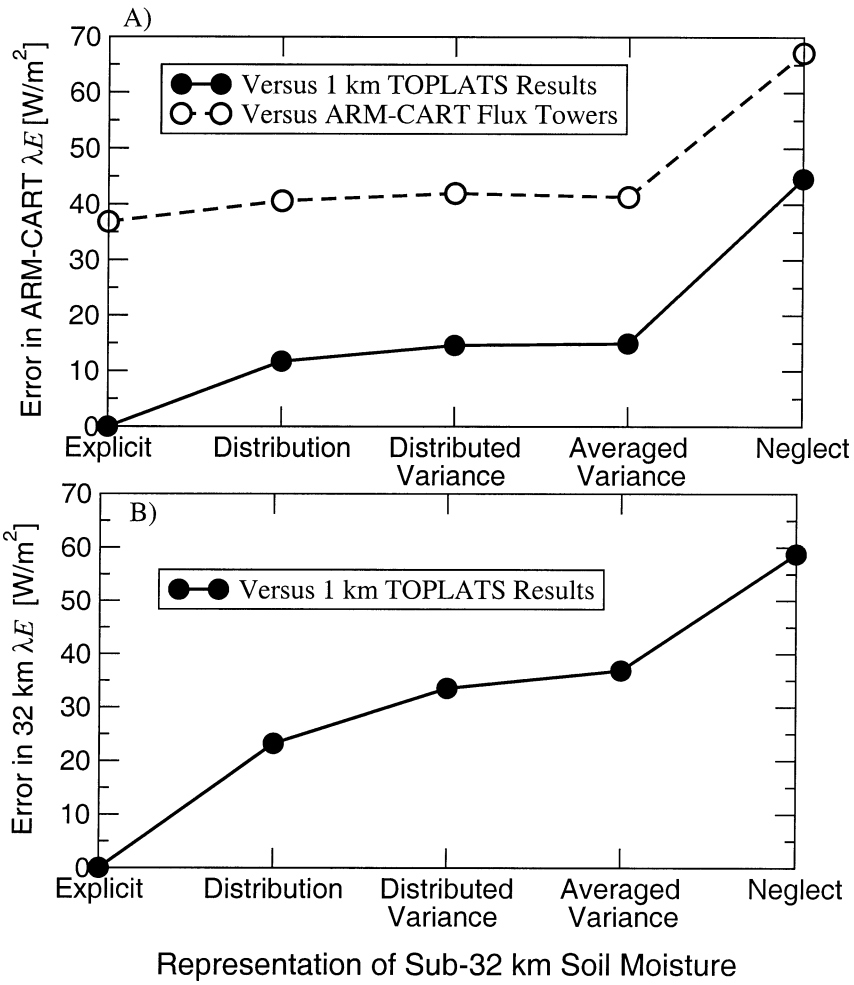

FIG. 9. Level of rms error in (a) ARM CART site–averaged and (b) 32-km noontime λE predictions associated with each of the strategies outlined in Fig. 8, plus the case of neglecting sub-32-km variability. Error is calculated relative to both TOPLATS predictions made with 1-km soil moisture data and validation data derived from EBBR flux tower observations within the ARM CART site.

is due to the inability of a statistical representation of soil moisture to represent the loss-of-correlation term defined in Eq. (3). However, subsequent degradation of subgrid information from a ''distribution'' to a ''local variance'' and from a ''local variance'' to an ''averaged variance'' description are associated with only minor (<3 W m^{-2}) increases in error relative to the sharp impact of moving from an ''averaged variance'' representation to the complete neglect of subgrid variability (29.6 W m^{-2}). A similar pattern is seen in Fig. 9a when TOPLATS predictions are compared to independent ARM CART flux tower observations.

Figure 9b demonstrates the value of each soil moisture representation for λE calculations at a finer scale (32 km). The reduction in accuracy associated with the transition from an ''averaged variance'' representation to complete neglect of subgrid-scale variability is less dramatic than for the coarser-scale correction shown in Fig. 9a. Nevertheless, knowledge of an averaged subgrid-scale soil moisture variance allows for correction of about one-third of the error in 32-km λE predictions associated with the complete neglect of sub-32-km soil moisture variability.

The large fraction of total error recovered by the ''averaged variance'' representation in Fig. 9 suggests that even simplistic statistical representations of subgrid soil moisture heterogeneity have value for efforts to predict grid-scale energy fluxes and offers support for the statistical representation of subgrid soil moisture variability employed by many land surface models (Famiglietti and Wood 1994a; Wetzel and Boone 1995).

c. Downscaling based on spatial scaling

Figure 10 examines the scaling structure of a single surface soil moisture field generated by TOPLATS over

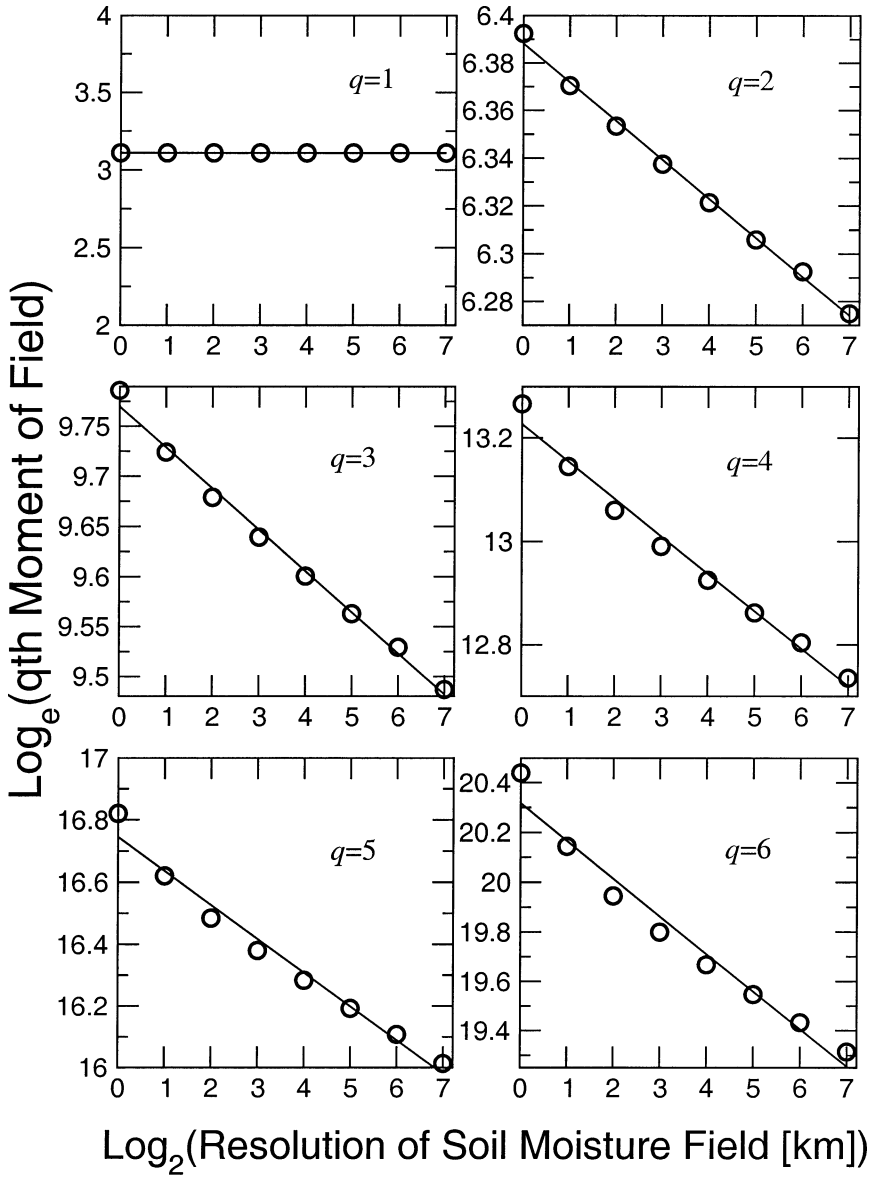

FIG. 10. Log–log plots of statistical moment order q vs scale for a typical surface soil moisture image generated by TOPLATS. Plotted resolutions vary from 1 km (2^0 km) to 128 km (2^7 km).

the Red–Arkansas River basin. It plots $\langle \theta^q \rangle$ versus scale and least squares regression lines fit in log–log space to obtain estimates of the scaling exponents $K(q)$. Figures 11a and 11b plot the scaling exponents and correlation coefficients associated with such fits for TOPLATS-generated surface soil moisture imagery during the 1994 growing season. Simple scaling requires linearity in the relationship between $K(q)$ and q and a single value for $\partial K(q)/\partial q$ at all q. In contrast to this requirement, Fig. 10c demonstrates that $\partial K(q)/\partial q$ becomes smaller (more negative) as q increases. This multiscaling signature in TOPLATS-derived soil moisture fields is consistent with previous results for both modeled (Dubayah et al. 1997; Peters-Lidard et al. 2001) and remotely sensed (Dubayah et al. 1997; Hu et al. 1998) soil moisture fields. Trends observed with respect to overall hydrologic conditions in the basin are also consistent with those noted in Peters-Lidard et al. (2001). That is, the power-law relationship between scale and statistical moments is a stronger assumption during wet periods of the simulation, and multiscaling features (i.e., concavity in plots of scaling exponents versus moment) are more pronounced during relatively dry periods.

The relatively strong power-law behavior (i.e., log–log linearity) demonstrated in Figs. 10 and 11 provides some confidence for applying the downscaling procedure shown in Fig. 4. The distinction between multi- and simple scaling is of secondary interest here, since

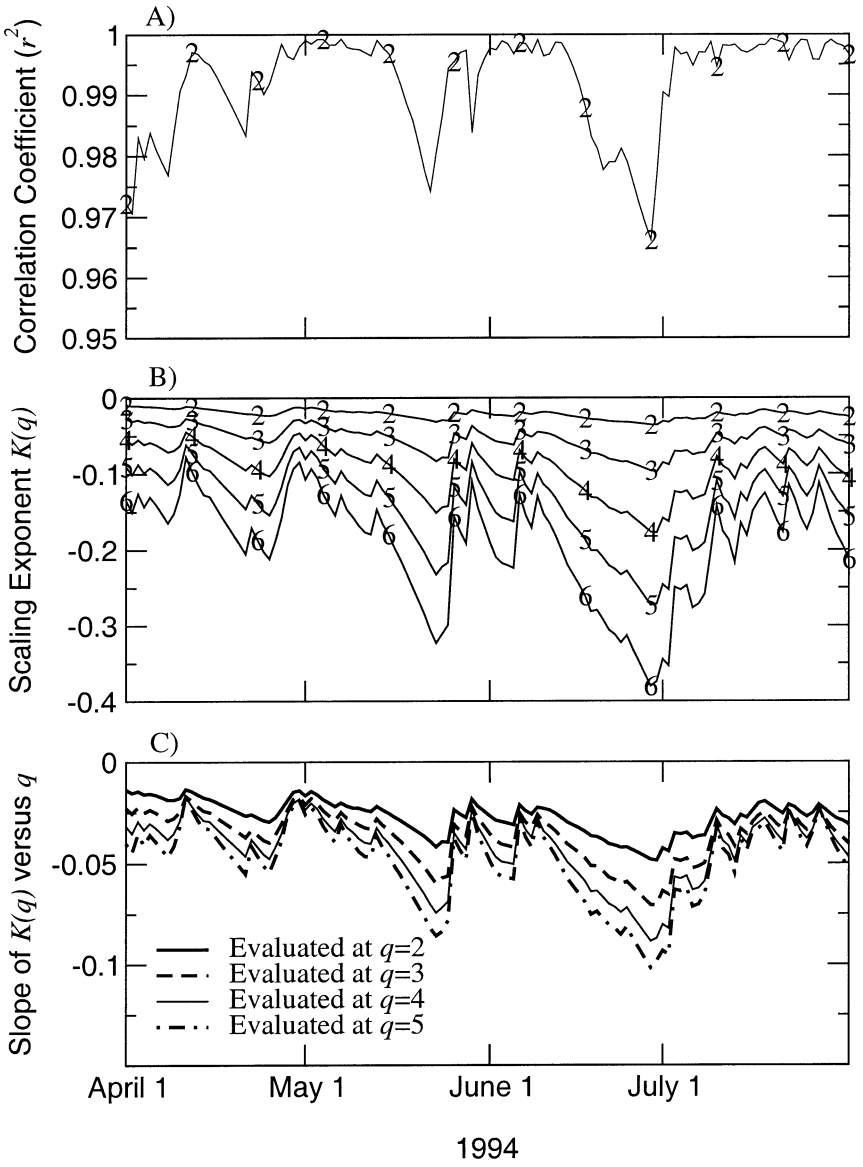

FIG. 11. For surface soil moisture fields simulated by TOPLATS and linear least squares fits in log–log space to the relationship between statistical moment order q and scale: (a) correlation coefficients (r^2) for $q = 2$, (b) the scaling exponent (i.e., log–log slope) $K(q)$ for $q = 2 \ldots 6$, and (c) the slope of $K(q)$ vs q evaluated at a range of q.

both predict a power-law relationship between statistical moments and scale that can be exploited using the procedure. Time series of actual versus predicted magnitudes of ARM CART site–averaged sub-32-km soil moisture variances are shown in Fig. 12. Predicted variances are derived from the application of the downscaling approach demonstrated in Fig. 4 to 32-km TOPLATS soil moisture imagery for the entire Red–Arkansas River basin. Actual variance magnitudes are taken directly from 1-km TOPLATS simulations of the ARM CART site. The downscaling procedure could be replicated for additional statistical moments, providing a more detailed estimation of subgrid statistics; however, Fig. 9 suggests that the benefits of more detailed statistical representations of subgrid variability are minimal.

For the 15-cm surface soil moisture zone, subgrid variance estimates shown in Fig. 12 are generally reasonable, except for dry periods in late May and late June, where the downscaling approach underpredicts subgrid variability. Log–log plots of the second statistical moment versus scale during this period exhibit an open-upward (positive) concavity, and scaling exponents fit at coarse (>32 km) scales tend to be larger (less negative) than scaling exponents fit at finer scales. The result is an underestimation of fine-scale, subgrid

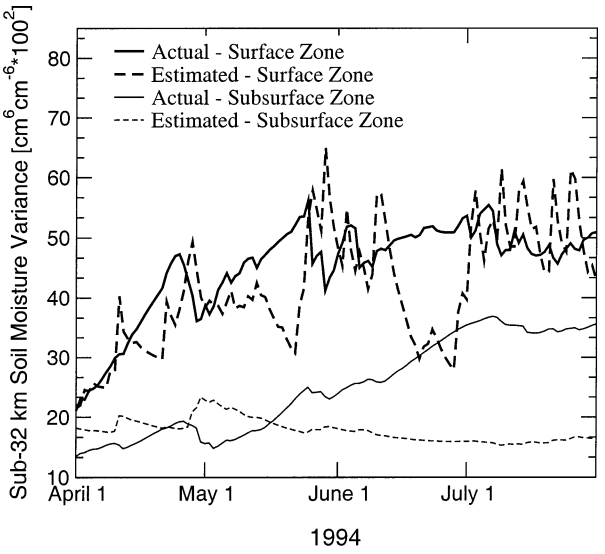

FIG. 12. Actual vs downscaled estimates of sub-32-km soil moisture variances for TOPLATS predictions within the ARM CART site.

variability when the fitted scaling exponent is extrapolated back to finer scales. Downscaling variability estimates for the more substantial subsurface zone appear adequate for April and May but are biased low during later portions of the summer. Clearly, the downscaling procedure provides only an approximate measure of subgrid variability. The critical question is whether such estimates are accurate enough to parameterize the nonlinearity term in Eq. (3) and correct TOPLATS surface energy flux predictions.

d. Correction of soil moisture aggregation impact using downscaling

Results in sections 5a–c lay the framework for a strategy to correct grid-scale surface energy flux predictions for the impact of nonresolved soil moisture heterogeneity. Figure 9 demonstrates that model estimates of λE can be substantially improved by knowledge of a single quantity—the average subgrid-scale soil moisture variance within the model domain—and Fig. 12 demonstrates the ability of the downscaling strategy to predict this quantity to within a reasonable accuracy.

Figure 13 plots accuracy gains in coarse-scale predictions of λE flux realized using an approach based on parameterization of the nonlinearity term in Eq. (3), assuming a beta probability distribution for subgrid-scale moisture heterogeneity and the daily estimation of a subgrid-scale soil moisture variance through the downscaling procedure outlined in Fig. 4. Because the approach attempts to close surface energy flux calculations for the impact of nonresolved soil moisture heterogeneity, it will be referred to as the ''downscaling closure model.'' When compared to ARM CART flux tower observations, the model recovers about half of the error (15.7 out of 30.3 W m^{-2}) associated with the aggregation of soil moisture (i.e., moving from an ''explicit'' to ''neglect'' representation in Fig. 13a). For finer-scale (32 km) λE calculations the downscaling closure model is less effective and corrects slightly more than one-quarter (16.8 out of 58.7 W m^{-2}) of the aggregation error (Fig. 13b). Of course, impacts associated with the aggregation of soil moisture represent only one source of error in TOPLATS surface energy predictions derived from 32-km soil moisture data. When both aggregation and underlying TOPLATS model errors are considered, the closure strategy reduces the total rms difference between ARM CART site–averaged model predictions and EBBR flux tower observations by slightly less than one-quarter (67.1 to 51.5 W m^{-2} in Fig. 13a).

Corrected TOPLATS results for other soil moisture resolutions are examined in Fig. 14 along with results associated with the uncorrected insertion of coarse-scale soil moisture imagery. Also plotted in Fig. 14 are error magnitudes associated with representing subgrid soil moisture variability using a fitted beta distribution. The figure allows for decomposition of the error associated with application of the downscaling closure model into various sources. For the 51.5 W m^{-2} error associated with the calculation of ARM CART site–scale λE using 32-km soil moisture data and the downscaling closure model, 36.9 W m^{-2} is associated with model (TOPLATS) and/or validation error, 6.5 W m^{-2} with degrading soil moisture variability within a 32-km grid cell from an explicit to a statistical representation (i.e., statistical representation error), and 8.1 W m^{-2} is attributable to the imperfect statistical description of soil moisture provided by the downscaling model (i.e., downscaling model error). The ''downscaling model error'' noted in Fig. 14 is a direct consequence of inaccuracies in the downscaling approach seen in Fig. 12, while the ''statistical representation error'' is introduced by the neglect of the loss-of-correlation term in the downscaling closure model.

The decrease in error for downscaling closure model results seen between 16 and 64 km in Fig. 14 is somewhat counterintuitive and is likely due to a spurious cancellation of biases. Downscaled estimates of variances within 64-km grid cells are biased high because of a slight break in the scaling of the TOPLATS-simulated soil moisture fields between 64 and 128 km. This overestimation of subgrid variability in turn causes an overestimation of the nonlinearity term in Eq. (3). However, the high bias of the nonlinearity term cancels a portion of the low bias associated with the neglect of the loss-of-correlation term and actually improves closure model results. In addition, at fine scales ($<$4 km) distributions of subgrid 1-km fields become less continuous and therefore less amenable to fitting using a smooth, unimodal beta probability distribution. This difficulty is reflected in the slight increase in error associated with a fitted beta-distribution representation of subgrid soil moisture at fine grid scales.

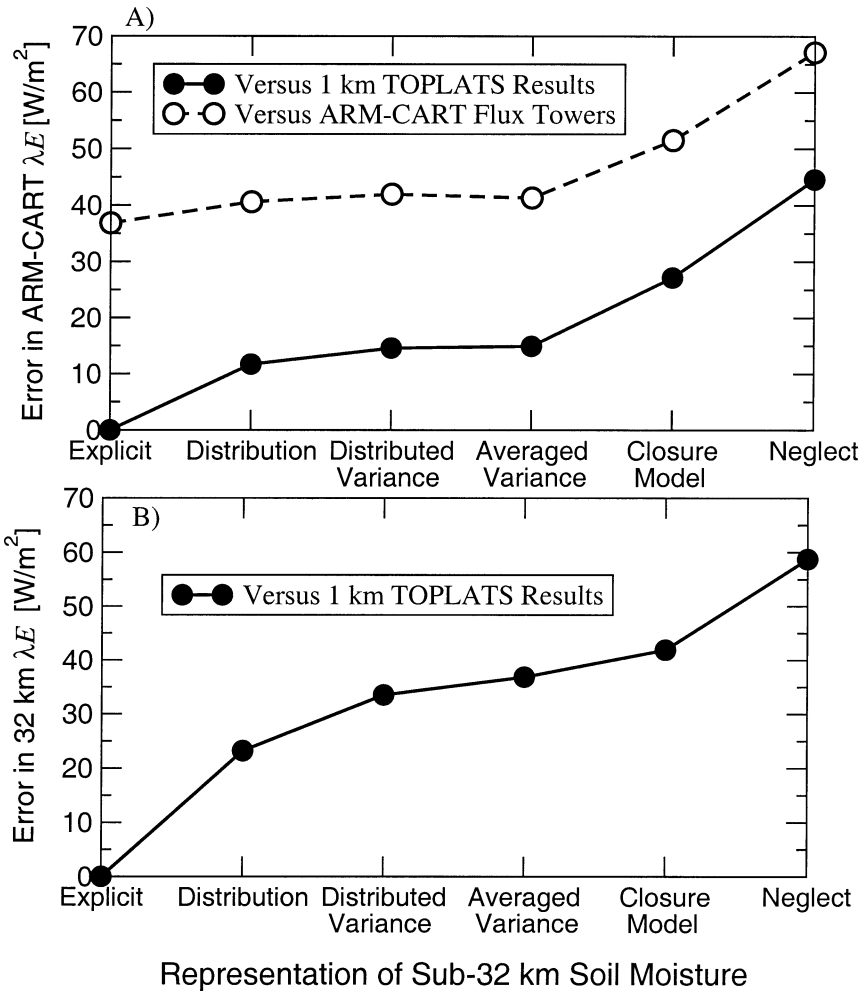

FIG. 13. Level of rms error in (a) ARM CART site–averaged and (b) 32-km noontime λE predictions associated with each of the strategies shown in Fig. 9, and the downscaling closure model presented in Fig. 4.

6. Discussion and conclusions

This analysis concerns itself solely with the impact of spatially aggregating soil moisture on the prediction of large-scale surface energy fluxes. Analogous concerns about the impact of averaging land surface parameters and the dynamic impacts of smoothing land surface heterogeneity are not considered. The emphasis on inserting coarse-scale (>30 km) observations into an otherwise fine-scale (1 km) model is made relevant by current trends in large-scale modeling capabilities and the availability of high-resolution land surface datasets. High-resolution vegetation, soil, and topographic maps are increasingly available at global and continental scales. Reflecting this availability, real-time land surface modeling on an ⅛° (~15 km) grid for North America is currently being performed as part of the North American Land Data Assimilation Scheme (NLDAS) project and on a ¼°–⅛° grid for all land north of 60°S within the Global Land Data Assimilation Scheme (GLDAS) project (details online at http://ldas.gsfc.nasa.gov). Even finer grid scales should be feasible in the near future. In contrast, the resolution of next-generation passive radiometers designed to measure soil moisture from space is unlikely to fall below 10–30 km even if innovative antennae design strategies are employed (Jackson et al. 1999).

The value of such coarse-scale soil moisture observations for surface energy flux prediction is contingent upon both the magnitude of the soil moisture aggregation effect and the ease with which this effect can be corrected using downscaling techniques. For the particular soil moisture/evapotranspiration formulation employed in TOPLATS (see Fig. 6 and section 5a), spatial smoothing of soil moisture has a profound impact on TOPLATS surface energy flux predictions made within the SGP ARM CART region during June and July 1994 (Fig. 5). However, results in Fig. 9 suggest that a downscaling strategy for soil moisture need not capture all

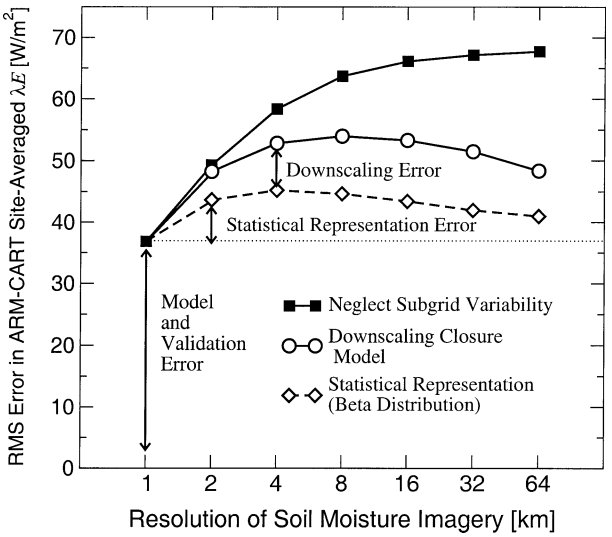

FIG. 14. Level of rms error in ARM CART site–averaged λE predictions associated with various representations of subgrid soil moisture heterogeneity for a range of grid scales. The error associated with the downscaling closure model (open circles) is composed of error in the downscaling procedure (Fig. 12), error associated with a statistical representation of subgrid soil moisture variability (Fig. 5b), and underlying model validation errors.

subgrid information in order to effectively compensate energy flux predictions for this error. In fact, a large fraction of the error associated with neglecting subgrid-scale soil moisture variability can be corrected using a single, domain-averaged, measurement of subgrid soil moisture variance. This result demonstrates the general feasibility of effective correction strategies by lowering the complexity requirements for descriptions of subgrid-scale soil moisture heterogeneity down to levels potentially obtainable using downscaling procedures.

This analysis also expands upon work by Dubayah et al. (1997) and Peters-Lidard et al. (2001) by assessing the spatial scaling properties of TOPLATS-simulated soil moisture fields for a larger spatial and temporal domain and demonstrating the degree to which the downscaling strategy shown in Fig. 4 is applicable to the simulated soil moisture fields. As in this previous work, results suggest that the simulated surface soil moisture fields consistently exhibit multiscaling behavior characterized by log–log linearity in $\langle \theta_\lambda^q \rangle$ versus scale λ and concavity in the relationship between $K(q)$ and q (Fig. 10).

Despite the general strength of a power-law relationship between second statistical moments and scale (Fig. 11), the downscaling procedure demonstrated in Fig. 4 provides a simplified, and at times inaccurate, representation of subfootprint-scale soil moisture heterogeneity (Fig. 12). However, utilizing the imperfect description it provides, within a probability density function (PDF) representation of subgrid variability, is clearly superior to the typical strategy of assuming zero subgrid variance and applying a point-scale model to coarse-scale information (Fig. 13). In fact, for footprint scales greater than 16 km, the downscaling closure model corrects roughly half of the model error associated with the aggregation of soil moisture data (Fig. 14). The ability to correct such aggregation-based errors is a key consideration for assessing the degree to which poor spatial resolution compromises the value of soil moisture observations from space.

The primary advantage of a downscaling procedure based on spatial scaling lies in its simplicity and ability to predict fine-scale variability in the absence of ancillary data or modified model calibration. Because it requires no additional model parameters, any benefit to model accuracy need not be balanced against concerns about increased model complexity. That said, a wide range of more complex downscaling procedures are possible. One particularly promising strategy is combining high-resolution land surface data (e.g., land cover or soil texture) and coarse-scale remotely sensed soil moisture imagery using variational data assimilation to recover subfootprint-scale heterogeneity in remotely sensed soil moisture fields (Reichle et al. 2001). This technique allows for recovery of subfootprint-scale cross correlation between land surface properties and soil moisture and, consequently, correction for a portion of the loss-of-correlation term in Eq. (3).

The coarse spatial resolution at which current antennae technology allows for the remote observation of soil moisture from space poses a challenge for efforts by hydrologists to demonstrate the value of a spaceborne sensor designed exclusively for the measurement of surface soil moisture. While aggregation effects surrounding the coarse-scale retrieval and insertion of soil moisture imagery into land surface models are potentially large, prospects for remediation of these errors through simplistic correction strategies appear quite good. The ease with which aggregation errors can be corrected suggests that the value of remotely sensed soil moisture observations for large-scale energy flux prediction is not irreparably compromised by poor horizontal sensor resolution.

Acknowledgments. This research was supported in part through NASA Grants NAG8-1517 and NAG5-6494. Data were obtained from the Atmospheric Radiation Measurement (ARM) Program sponsored by the U.S. Department of Energy.

REFERENCES

Avissar, R., 1992: Conceptual aspects of a statistical–dynamical approach to represent landscape subgrid-scale heterogeneities in atmospheric models. *J. Geophys. Res.*, **97,** 2729–2742.

——, and T. Schmidt, 1998: An evaluation of the scale at which ground-surface heat flux patchiness affects the convective boundary layer using a large-eddy simulation model. *J. Atmos. Sci.*, **55,** 2666–2689.

Betts, A. K., and A. C. M. Beljaars, 1993: Estimation of effective

roughness length for heat and momentum from FIFE data. *Atmos. Res.*, **30,** 251–261.

Blöschl, G., and M. Sivipalan, 1995: Scale issues in hydrological modeling: A review. *Scale Issues in Hydrological Modeling*, M. Sivipalan and J. D. Kalma, Eds., John Wiley and Sons, 9–48.

Boulet, G., J. D. Kalma, I. Braud, and M. Vauclin, 1999: An assessment of effective land surface parameterisation in regional-scale water balance studies. *J. Hydrol.*, **217,** 225–238.

Brutsaert, W., 1982: *Evaporation Into the Atmosphere*. D. Reidel, 299 pp.

Choudhury, B. J., and C. A. Federer, 1984: Some sensitivity results for corn canopy temperature and its spatial variation induced by soil hydraulic heterogeneity. *Agric. For. Meteor.*, **31,** 297–317.

——, and S. B. Idso, 1985: Evaluating plant and canopy resistances of field grown wheat from concurrent diurnal observations of leaf water potential, stomatal resistance, canopy temperature and evapotranspiration flux. *Agric. For. Meteor.*, **34,** 67–76.

Cosby, B. J., G. M. Hornberger, R. B. Clapp, and T. R. Ginn, 1984: A statistical exploration of the relationships of soil water characteristics to the physical properties of soils. *Water Resour. Res.*, **20,** 682–690.

Crow, W. T., E. F. Wood, and R. Dubayah, 2000: Potential for downscaling soil moisture maps derived from spaceborne imaging radar data. *J. Geophys. Res.*, **105,** 2203–2212.

——, M. Drusch, and E. F. Wood, 2001: An Observation System Simulation Experiment (OSSE) for the impact of land surface heterogeneity on AMSR-E soil moisture retrieval. *IEEE Trans. Geosci. Remote Sens.*, **39** (8), 1622–1631.

Desborough, C. E., 1997: The impact of root weighting on the response of transpiration to moisture stress in land surface schemes. *Mon. Wea. Rev.*, **125,** 1920–1930.

Diak, G. R., and C. Gautier, 1983: Improvements to a simple physical model for estimating insolation from GOES data. *J. Climate Appl. Meteor.*, **22,** 505–508.

Dingman, S. L., 1994: *Physical Hydrology*. Prentice Hall, 575 pp.

Doran, J. C., J. M. Hubbe, J. C. Liljigren, W. J. Shaw, G. J. Collatz, D. R. Cook, and R. L. Hart, 1998: A technique for determining the spatial and temporal distributions of surface fluxes of heat and moisture over the Southern Great Plains Cloud and Radiation Testbed. *J. Geophys. Res.*, **103,** 6109–6121.

Drusch, M., E. F. Wood, and R. Lindau, 1999a: The impact of the SSM/I antenna gain function on land surface parameter retrieval. *Geophys. Res. Lett.*, **26,** 3481–3484.

——, ——, and C. Simmer, 1999b: Up-scaling effects in passive microwave remote sensing: ESTAR 1.4 GHz measurements during SGP'97. *Geophys. Res. Lett.*, **26,** 879–882.

Dubayah, R., E. F. Wood, and D. Lavalee, 1997: Multiscaling analysis in distributed modeling and remote sensing: An application using soil moisture. *Scale, Multiscaling, Remote Sensing, and GIS*, M. F. Goodchild and D. A. Quattrochi, Eds., Cambridge University Press, 93–111.

Famiglietti, J. S., and E. F. Wood, 1994a: Application of multiscale water and energy balance models on a tall grass prairie. *Water Resour. Res.*, **30,** 3079–3093.

——, and ——, 1994b: Multiscale modeling of spatially variable water and energy balance processes. *Water Resour. Res.*, **30,** 3061–3078.

——, and ——, 1995: Effects of spatial variability and scale on areally averaged evapotranspiration. *Water Resour. Res.*, **31,** 699–712.

——, and Coauthors, 1999: Ground-based investigation of soil moisture variability within remote sensing footprints during the Southern Great Plains 1997 (SGP97) Hydrology Experiment. *Water Resour. Res.*, **35,** 1839–1851.

Fast, J. D., and M. D. McCorcle, 1991: The effect of heterogeneous soil moisture on a summer baroclinic circulation in the central United States. *Mon. Wea. Rev.*, **119,** 2140–2168.

Feddes, R. A., and P. E. Rijtema, 1972: Water withdrawal by plant roots. *J. Hydrol.*, **17,** 35–59.

Federer, C. A., 1979: A soil–plant–atmosphere model for transpiration and availability of soil water. *Water Resour. Res.*, **15,** 555–562.

Gao, W., R. L. Coulter, B. M. Lesht, J. Qiu, and M. L. Wesley, 1998: Estimating clear-sky regional surface fluxes in the Southern Great Plains Atmospheric Radiation Measurement site with ground measurements and satellite observations. *J. Appl. Meteor.*, **37,** 5–22.

Giorgi, F., and R. Avissar, 1997: Representation of heterogeneity effects in earth system modeling: Experience from land surface modeling. *Rev. Geophys.*, **35,** 413–438.

Gupta, H. V., L. A. Bastidas, S. Sorooshian, W. J. Schuttleworth, and Z. L. Zhang, 1999: Parameter estimation of a land surface scheme using multicriteria methods. *J. Geophys. Res.*, **104,** 19 491–19 503.

Gupta, V. K., and E. Waymire, 1990: Multiscaling properties of spatial rainfall and river flow distributions. *J. Geophys. Res.*, **95,** 1999–2009.

Hillel, D., 1980: *Fundamentals of Soil Physics.* Academic Press, 413 pp.

Hu, Z., Y. Chen, and S. Islam, 1998: Multiscaling properties of soil moisture images and decomposition of large- and small-scale features using wavelet transforms. *Int. J. Remote Sens.*, **19,** 2451–2467.

Hudlow, M. D., J. A. Smith, M. L. Walton, and R. C. Shedd, 1991: NEXRAD: New era in hydrometeorology. *Hydrological Applications of Weather Radar*, I. Cluckie and C. Colliers, Eds., Ellis Horwood, 602–612.

Jackson, T. J., D. M. Le Vine, A. Y. Hsu, A. Oldak, P. J. Starks, C. T. Swift, J. D. Isham, and M. Haken, 1999: Soil moisture mapping at regional scales using microwave radiometry: The Southern Great Plains Hydrology Experiment. *IEEE Trans. Geosci. Remote Sens.*, **37,** 2136–2151.

Jacquemin, B., and J. Noilhan, 1990: Sensitivity study and validation of a land-surface parameterization using the HAPEX–MOBILHY data set. *Bound.-Layer Meteor.*, **52,** 93–134.

Jarvais, P. G., 1976: The interpretation of the variations in leaf water potential and stomatal conductance found in canopies in the field. *Philos. Trans. Roy. Soc. London*, **273B,** 563–610.

Kondo, J., 1971: Relationship between the roughness coefficient and other aerodynamic parameters. *J. Meteor. Soc. Japan*, **49,** 120–124.

Koster, R. D., M. J. Suarez, and M. Heiser, 2000: Variance and predictability of precipitation at seasonal–to–interannual time scales. *J. Hydrometeor.*, **1,** 26–46.

Kustas, W. P., and T. J. Jackson, 1999: The impact on area-averaged heat fluxes from using remotely sensed data at different resolutions: A case study with Washita '92 data. *Water Resour. Res.*, **35,** 1539–1550.

Le Vine, D. M., A. J. Griffis, C. T. Swift, and T. J. Jackson, 1994: ESTAR: A synthetic aperture microwave radiometer for remote sensing applications. *Proc. IEEE*, **82,** 1787–1801.

Lynn, B. H., D. Rind, and R. Avissar, 1995: The importance of mesoscale circulations generated by subgrid-scale landscape heterogeneities in general circulation models. *J. Climate*, **8,** 191–205.

Njoku, E. G., S. J. Hook, and A. Chehbouni, 1996: Effects of surface heterogeneity on thermal remote sensing of land parameters. *Scaling up in Hydrology Using Remote Sensing*, J. B. Stewart et al., Eds., John Wiley and Sons, 19–39.

Peters-Lidard, C. D., M. S. Zion, and E. F. Wood, 1997: A soil–vegetation–atmosphere transfer scheme for modeling spatially variable water and energy balance processes. *J. Geophys. Res.*, **102,** 4303–4324.

——, E. Blackburn, X. Liang, and E. F. Wood, 1998: The effect of soil thermal conductivity parameterization on surface energy fluxes and temperatures. *J. Atmos. Sci.*, **55,** 1209–1224.

——, F. Pan, and E. F. Wood, 2001: A re-examination of modeled and measured soil moisture spatial variability and its implications for land surface modeling. *Adv. Water Resour.*, **24,** 1069–1083.

Pielke, R. A., 1984: *Mesoscale Meteorological Modeling.* Academic Press, 612 pp.

Rawls, W. J., D. L. Brakensiek, and K. E. Saxton, 1982: Estimation of soil water properties. *Trans. ASAE,* **25,** 1316–1320.

Reichle, R., D. Entekhabi, and D. B. McLaughlin, 2001: Downscaling of radiobrightness measurements for soil moisture estimation: A four-dimensional variational data assimilation approach. *Water Resour. Res.,* **37,** 2353–2364.

Rodriguez-Iturbe, I., G. K. Vogel, R. Rigon, D. Entekhabi, F. Castelli, and A. Rinaldo, 1995: On the spatial organization of soil moisture fields. *Geophys. Res. Lett.,* **22,** 2757–2760.

Sellers, P. J., and Coauthors, 1995: Effects of spatial variability in topography, vegetation cover, and soil moisture on area-averaged surface fluxes: A case study using the FIFE 1989 data. *J. Geophys. Res.,* **100,** 25 607–25 629.

Seth, A., and F. Giorgi, 1996: A three-dimensional study of organized mesoscale circulations induced by vegetation. *J. Geophys. Res.,* **101,** 18 561–18 667.

Stull, R. B., 1995: *Meteorology Today for Scientists and Engineers.* West Publishing Company, 385 pp.

Weaver, C. P., and R. Avissar, 2001: Atmospheric disturbances caused by human modification of the landscape. *Bull. Amer. Meteor. Soc.,* **82,** 269–281.

Wetzel, P. J., and J. Chang, 1987: Concerning the relationship between evapotranspiration and soil moisture. *J. Climate Appl. Meteor.,* **26,** 18–27.

——, and ——, 1988: Evapotranspiration from nonuniform surfaces: A first approach for short-term numerical weather prediction. *Mon. Wea. Rev.,* **116,** 600–621.

——, and A. Boone, 1995: A Parameterization for Land–Atmosphere–Cloud Exchange (PLACE): Documentation and testing of a detailed process model of the partly cloudy boundary layer over heterogeneous land. *J. Climate,* **8,** 1810–1837.

Wood, E. F., 1997: Effects of soil moisture aggregation on surface evaporation fluxes. *J. Hydrol.,* **190,** 397–412.

——, and Coauthors, 1998: The Project for Intercomparison of Land-Surface Parameterization Schemes (PILPS) Phase 2(c) Red–Arkansas River basin experiment. 1. Experiment description and summary intercomparison. *Global Planet. Change,* **19,** 115–135.

Zhong, S., and J. C. Doran, 1997: A study of the effects of spatially varying fluxes on cloud formation and boundary layer properties using data from the Southern Great Plains Cloud and Radiation Testbed. *J. Climate,* **10,** 327–341.

——, and ——, 1998: An evaluation of the importance of surface flux variability on GCM-scale boundary-layer characteristics using realistic meteorological and surface forcing. *J. Climate,* **11,** 2774–2788.